

TNO report

R11278

**Ensemble-based Subsidence Interpretation
and Prediction ESIP: Technical Reference
Manual**

Princetonlaan 6
3584 CB Utrecht
P.O. Box 80015
3508 TA Utrecht
The Netherlands

www.tno.nl

T +31 88 866 42 56
F +31 88 866 44 75

Date	26 January 2017
Author(s)	T.G.G. Candela, P.A. Fokker, D. Hegen
Number of pages	27 (incl. appendices)
Number of appendices	1
Sponsor	Nederlandse Aardolie Maatschappij B.V.
Project name	Ontwikkeling probabilistische model workflow t.b.v. voorspelling van bodemdaling
Project number	060.20904

All rights reserved.

No part of this publication may be reproduced and/or published by print, photoprint, microfilm or any other means without the previous written consent of TNO.

In case this report was drafted on instructions, the rights and obligations of contracting parties are subject to either the General Terms and Conditions for commissions to TNO, or the relevant agreement concluded between the contracting parties. Submitting the report for inspection to parties who have a direct interest is permitted.

© 2017 TNO

Contents

1	Introduction	3
2	General Description	4
3	Upscaling	6
4	Compaction models	8
4.1	Linear model	8
4.2	Bilinear model	8
4.3	Time decay model	9
4.4	Rate type isotach model	9
4.5	Interpolation	11
5	From influence functions to ground motions	12
5.1	Exponential influence function	12
5.2	Physic-based influence function	12
6	Double differences	15
7	Generating the prior ensemble	16
8	Geodetic data	17
9	Conditioning of the models with the data	18
9.1	Red-Flag approach	19
9.2	Ensemble Smoother approach	20
10	Assessment	24
11	References	25
	Confidential Appendix: Sampling scheme	27

1 Introduction

During gas extraction, the reservoir pressure often decreases and which leads to compaction of the reservoir. This reduction in volume at reservoir depth may induce surface subsidence [Doornhof, 1992]. Ongoing production may cause further ongoing subsidence even after production has stopped [van Thienen-Visser et al., 2015], and this may have consequences for the environment and for human activities near the area at surface where the gas production takes place [van Thienen-Visser et al., 2012]. To judge whether such effects take place and to be able to study consequences of actions, subsidence forecasts connected to gas production are required. TNO has been contracted by NAM for developing and implementing a workflow that addresses this requirement.

The current report serves as technical reference manual and presents the main ingredients of this workflow, and which has been named the Ensemble based Subsidence Interpretation and Prediction tool, in the sequel referred to as **ESIP**. After a further introduction given in the next chapter, the chapters 3-10 present (i) the details of the methods applied in the workflow and (ii) the outputs generated.

2 General Description

The production of gas from a reservoir is accompanied by uncertainties in the subsurface parameters and processes. For any forecasting method (e.g. of surface subsidence due to gas production) to be useful, this uncertainty must be taken into account, and, where possible, reduced. In many scientific realms where uncertainties are abundant, like weather forecasting, it has become clear that a probabilistic ensemble approach is a fruitful method for doing so (e.g. [Reggiani and Weerts, 2008], [Jaynes, 2003], [Evensen, 2003], [Emerick and Reynolds, 2013]). Therefore, a probabilistic ensemble approach has been chosen as one of the main ingredients for **ESIP**. Furthermore, as a second main ingredient, reduction of the uncertainty is achieved by incorporating surface movement measurements.

ESIP starts from two pieces of information:

1. an ensemble of reservoir flow model simulation results (pressure scenarios through time, and
2. ground motions measurements provided by the geodetic module [Van Leijen et al., 2017].

From the reservoir flow simulations, **ESIP** calculates compaction and subsidence using a geomechanical simulator. To circumvent the effect of the choice of references in time and space, the ground motion measurements are translated to double difference observations and the corresponding covariance matrix. Finally, **ESIP** performs a model conditioning and produces improved ground motion predictions. A schematic representation of the **ESIP** workflow steps is provided in Figure 1.

ESIP takes advantage of a-priori knowledge mapped out in the reservoir models driving input parameters and in the parameters of the geomechanical models. This way, given the ensemble of reservoir flow simulations received as user inputs, **ESIP** generates ensembles of modelled surface movements by stochastically selecting values in the prior distributions of the driving input parameters of the geomechanical forward models. The results are provided in the form of double differences since the surface movement measurements are also given in that format. Then, these ensembles of prior double differences are conditioned using a confrontation with the data to refine the predictions. Finally, the updated or conditioned models are propagated to the future, utilizing the projected production scenarios. Forecasts of surface movement are given as well in the form of an ensemble of double differences predictions to facilitate direct comparison with future measurements.

ESIP approaches intend to be “generic” in the sense that it is not specifically tailored for application to a specific reservoir. Hence, **ESIP** may be applied to any producing reservoir of interest, but of course the limitations of the methods may prevent **ESIP** to be suitable for specific applications. One of such limitations is that so far **ESIP** is only able to act on reservoir flow simulation results obtained with one specific reservoir simulator. In the sequel of this report several further limitations are being brought to the attention of the reader.

Based on synthetic reservoir flow simulations generated with the Shell propriety reservoir simulator MoReS the **ESIP** approaches have been demonstrated. This synthetic gas reservoir model mimics all the complexities of many real cases (such

as faults, aquifer connected), and is thus well suited for testing purposes since the model geometry (reservoir/aquifer boundaries) and the a-priori uncertainties of each of the model parameters are well constrained. In our synthetic scenario, however, the geodetic module is not exactly used in the same way as in the workflow described below. Instead it is used to create a proper synthetic data covariance matrix and data noise that is consistent with it. The synthetic data correspond to one member of one of the ensembles of double differences generated for each type of compaction model, with the noise added. A full description of this synthetic field and the study based on it is beyond the scope of the present document and will be deferred. The remainder of the present report will detail the background of the different steps in the **ESIP** workflow.

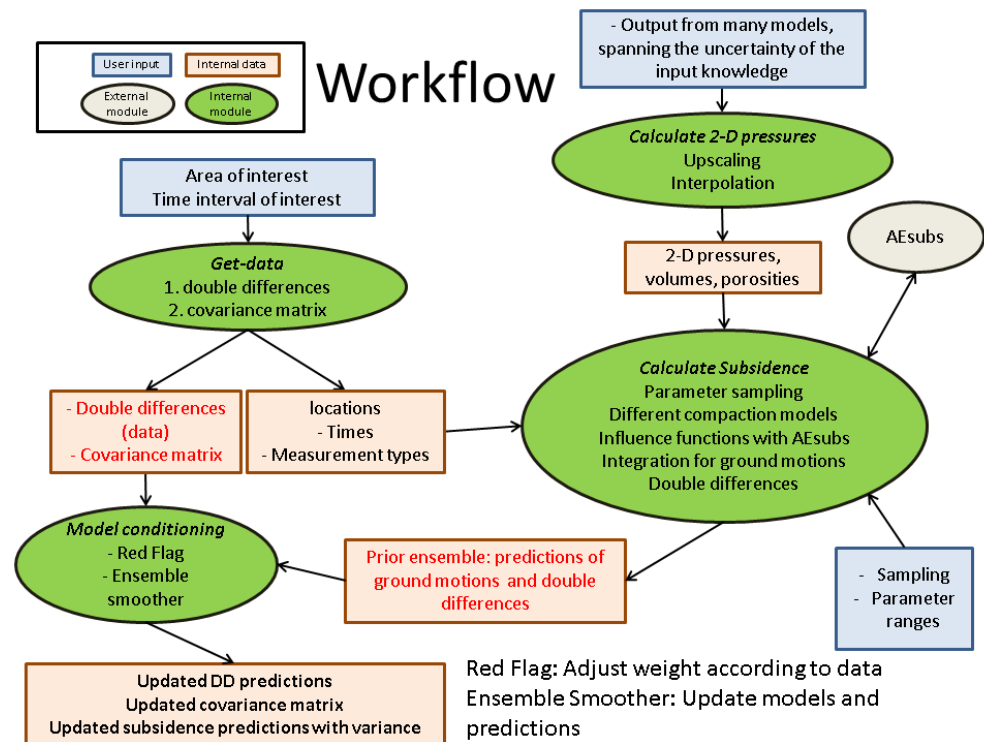


Figure 1: Schematic representation of **ESIP** workflow steps

3 Upscaling

The output of the MoReS reservoir simulator is a pressure field on a detailed 3-D grid. The ensemble-based approach followed in **ESIP** precludes the use of such full-field grids in the geomechanical and geodetic analysis. Therefore, all 3-D pressure fields need to be up-scaled as one of the first steps.

The upscaling procedure consists of two steps, first the *vertical* averaging of the pressure in the reservoir layers, and as second step the *horizontal* averaging over a coarser grid. This averaging process is justified by the fact that the distribution of compaction over an upscaled cell in a thin and deep reservoir has a limited effect on the surface subsidence [Geertsma, 1973].

The upscaling needs to be performed such that the amount of compaction for the upscaled 2-D grid and the initial layered 3-D grid is identical. Therefore, the *vertical* and *horizontal* averaging of the 3-D pressure field need to be weighted, to take into account the variability in compaction between each individual grid block of the reservoir model. The variability in compaction is controlled by differences in pressures, volumes, and porosities between each grid block. The *vertically* averaged pressures P_{av} , volumes V_{tot} , porosities ϕ_{av} and grid block center positions X_{av} and Y_{av} for one vertical column of the 3-D grid can be expressed as:

$$P_{av} = \frac{\sum_{k=1}^n C_{mk}(\phi_k) \cdot P_k \cdot V_k}{C_m(\phi_{av}) \cdot V_{tot}} \quad (1)$$

$$V_{tot} = \sum_{k=1}^n V_k \quad (2)$$

$$\phi_{av} = \sum_{k=1}^n \phi_k \cdot \frac{V_k}{V_{tot}} \quad (3)$$

$$X_{av} = \sum_{k=1}^n X_k \cdot \frac{V_k}{V_{tot}} \quad (4)$$

$$Y_{av} = \sum_{k=1}^n Y_k \cdot \frac{V_k}{V_{tot}} \quad (5)$$

In equation (1) $C_{mk}(\phi_k)$ corresponds to the compaction coefficient of one grid block as a function of its porosity, pressure, and time. This specific relationship is normally constrained by uniaxial experiments. The volume $C_{mk}(\phi_k)$ considered for each individual grid block is the net volume, that is only including reservoir parts.

After this first step of *vertical* upscaling we have a 2-D irregular fine grid of P_{av} , ϕ_{av} , V_{tot} at upscaled positions (X_{av}, Y_{av}) .

The second step of the upscaling consists in the *horizontal* averaging of pressures, volumes, and porosities of the 2-D fine grid (X_{av}, Y_{av}) falling within the limits of a 2-D regular coarse grid covering the area of the reservoir model. The regular coarse grid size can be flexible and is typically between 500-1000m. In order to maintain the same amount of compaction before and after upscaling, the same averaging procedure needs to be followed as for the *vertical* averaging in equations (1) – (5). After this second step of *horizontal* upscaling we end-up with a 2-D coarse irregular grid with new (x_{av}, y_{av}) positions, pressures, volumes, and porosities.

Following this vertical upscaling approach, each reservoir column is taken based on the grid block numbering only, i.e. the numbering that applies to the grid dimension that likely aligns with the vertical thickness direction of the reservoir. In doing so, one assumes the reservoir column as sub-vertical. Close-by low dipping faults, this vertical upscaling approach may not be suitable, since the reservoir column is more likely to depart from the verticality. Also, as a further limitation it is being remarked that this **ESIP** upscaling approach is not yet capable of dealing with detailed 3-D grids as obtained from MoReS, notably when local grid refinement has been applied.

4 Compaction models

Four types of compaction models have been selected for translating the pressure depletions in terms of compacted volume. These are the linear, the bilinear, the time decay, and the rate type model. Each compaction model as is described in the next four sections of this chapter intends to characterize the non-trivial and often non-linear relationship between pressure depletion and compaction of the rock volume. As should be clear from Figure 1 each such compaction model is applied by **ESIP** on the coarse 2-D grid obtained from the upscaling approach discussed in the previous chapter. This chapter concludes with a section on the interpolation of pressure data over time to serve as input for the different compaction models of **ESIP**.

4.1 Linear model

Assuming a linear relationship between pressure depletion and compaction, one can derive the compaction of each grid block as:

$$V_{comp}(x, y, t) = C_m(x, y) \cdot V(x, y) \cdot dP(x, y, t) \quad (6)$$

The compaction coefficient of the reservoir rock C_m is here again linked to the reservoir model porosity by the lab-derived polynomial relationship. Even if this linear model is often supported by uniaxial lab rock testing, it still remains to determine whether these experiments fully capture the full complexity of the reservoir compaction.

Only one material parameter C_m is needed for the linear compaction model, but the parameter can be position dependent due to its dependence on lithology and porosity.

4.2 Bilinear model

Subsidence data on top of gas fields in the Netherlands demonstrate a delay in the subsidence relative to the evolution of production and the associated pressure depletion [van Thienen-Visser et al., 2015]. The subsidence rate is slow at the early stage of reservoir depletion, and switches to a faster rate when a characteristic reservoir pressure has been reached. Assuming a purely elastic response of the layers surrounding the reservoir, this behavior can be modeled using two linear relationships between pressure depletion and reservoir rock compaction [NAM et al., 2015] as:

$$V_{comp_{pre}}(x, y, t) = C_{m_{pre}}(x, y) \cdot V(x, y) \cdot (P_0(x, y) - P(x, y, t)) \quad (7)$$

$$V_{comp_{post}}(x, y, t) = C_{m_{pre}}(x, y) \cdot V(x, y) \cdot (P_0(x, y) - P_{trans}(x, y)) + C_{m_{post}}(x, y) \cdot V(x, y) \cdot (P_{trans}(x, y) - P(x, y, t)) \quad (8)$$

where P_0 and P_{trans} respectively define the initial pressure before the start of production and the transition pressure. The first relationship should fit the slow subsidence rate at early stage using a low $C_{m_{pre}}$ value; the second relationship addresses the later-stage faster subsidence using a high value for $C_{m_{post}}$. The first linear relationship is used from the onset of pressure depletion up to the transition

pressure P_{trans} , whereas the second linear relationship is used for pressures higher than P_{trans} .

The two material parameters $C_{m_{pre}}$, $C_{m_{post}}$ and the pressure P_{trans} are required to compute the bilinear compaction.

4.3 Time decay model

The linear and bilinear models both failed explaining recent observations in the Netherlands of persistent subsidence even when production had stopped. A way to explain both the subsidence delay at the onset of production and the persistent subsidence at the arrest of pressure depletion is to evoke a time decay process. The background of this suggestion was the observation of the general diffusive behavior of many physical systems pushed into a disequilibrium high-energy state, which slowly decay to their low-energy equilibrium state [Mossop, 2012]. Such a diffusion-type process can be modeled using a convolution of a linear relationship between pressure depletion and reservoir rock compaction (as equation (6)) with an exponential time decay function:

$$V_{comp}(x, y, t) = C_m(x, y, t) \cdot V(x, y, t) \cdot dP(x, y, t) * \frac{1}{\tau} \exp\left[-\frac{t}{\tau}\right] \quad (9)$$

It is important to point out that the exponential time decay function and its characteristic time are not laboratory-based and that the underlying micro-mechanics controlling the time decay are still unknown. In addition, it is important to point out that this approach is assuming the purely elastic linear response of the rocks surrounding the reservoir rock. Indeed, the hypothesis of a visco-elastic salt layer overlaying the reservoir, and creeping in response to reservoir compaction, might lead to a similar time-dependence of the subsidence [NAM et al., 2015].

In order to compute the time decay compaction, the material parameter C_m and the characteristic time decay constant τ are required.

4.4 Rate type isotach model

Traditional uniaxial experiments are conducted at one single constant loading rate. [De Waal (1986)] ran a series of experiments changing the loading rate during the experiments. The motivation for this experimental design was to capture the rate dependence of sandstone compaction as previously observed for soft soil [Bjerrum, 1967]. [De Waal (1986)] demonstrated that a faster loading rate leads to stiffer response of the rock sample, that is a slower compaction rate. At a change of the loading rate, a first direct strain response is recorded followed by a more gradual response. These experimental observations might explain the subsidence behavior at the onset and arrest of production, which can be seen as changes in loading rate of the reservoir rocks.

Recently [Pruiksma et al. (2015)] reformulated and implemented the rate type compaction model of [De Waal (1986)] in order to model the transition from one loading rate to another (or a zero loading rate). Their new formulation is based on the linear isotach compaction model developed for soft soil [Den Haan, 2003]. Isotachs define lines of constant loading rate in a stress-strain diagram. At the change in loading rate, a first direct elastic strain ε_d response is observed, followed

by a more gradual creep strain ε_s response. Once the new constant loading rate is reached, this new path of linear compaction is eventually preserved.

The rate type isotach compaction in **ESIP** is derived from an explicit Euler finite-difference scheme keeping a constant time step Δt [Pruksma et al. (2015)]. To calculate the compaction of one grid block grid (x, y) the applied numerical scheme can be divided into 5 steps as follows:

1) From the current effective vertical stress $\sigma'(t)$ and strain $\varepsilon(t)$, calculate the creep strain rate as:

$$\dot{\varepsilon}_s(t) = \left(\frac{\varepsilon(t) - \varepsilon_0}{\sigma'(t)} - C_{m_d} \right) \dot{\sigma}'_{ref} \left(\frac{\varepsilon(t) - \varepsilon_0}{\sigma'(t) \cdot C_{m_{ref}}} \right)^{-1/b} \quad (10)$$

The vertical effective stress is derived from the reservoir depth and the mean density ρ_{mean} of the subsurface up to the reservoir top z_r as:

$$\sigma'(t) = (\rho_{mean} \cdot g \cdot z_r) - P(t) \quad (11)$$

At t_0 , that is at the onset of pressure depletion/production, the direct elastic strain $\varepsilon_d(t_0)$ and creep strain $\varepsilon_s(t_0)$ are both considered equal to zero, and thus total strain $\varepsilon(t_0)$ is set to zero.

The reference total strain is expressed as:

$$\varepsilon_0 = -C_{m_{ref}} \cdot \sigma'_{ref} \quad (12)$$

with the reference vertical effective stress $\sigma'_{ref} = \sigma'(t_0)$.

Three material parameters ($C_{m_{ref}}$, C_{m_d} , b) and one state parameter ($\dot{\sigma}'_{ref}$) are needed to compute the rate type compaction. The material parameters $C_{m_{ref}}$ and C_{m_d} are respectively the reference and direct compaction coefficients, where $C_{m_{ref}}$ is the compaction coefficient corresponding to the pre-depletion loading rate, and thus by definition quite high. Parameter C_{m_d} is dedicated to map out the direct effect at the change of loading rate. In the scenario of the change of loading rate due to the onset of pressure depletion, C_{m_d} is expected to be low in order to mimic the stiff response of the reservoir rocks.

2) The second step of the Euler scheme consists in calculating the increase in creep strain as:

$$\Delta \varepsilon_s = \dot{\varepsilon}_s(t) \cdot \Delta t \quad (13)$$

and update the creep strain as:

$$\varepsilon_s(t_{+1}) \rightarrow \varepsilon_s(t) + \Delta \varepsilon_s \quad (14)$$

3) The time is updated as $t_{+1} \rightarrow t + \Delta t$

4) Following a linear stress-strain relationship one can calculate the direct elastic strain as:

$$\varepsilon_d(t + \Delta t) = C_{m_d} \cdot (\sigma'(t + \Delta t) - \sigma'_{ref}) \quad (15)$$

5) Finally one can calculate the total cumulative strain as:

$$\varepsilon(t + \Delta t) = \varepsilon_s(t + \Delta t) + \varepsilon_d(t + \Delta t) \quad (16)$$

And the total cumulative compaction as:

$$V_{comp}(t + \Delta t) = -\varepsilon(t + \Delta t) \cdot V \quad (17)$$

with V the grid block net volume, assumed constant over time. Clearly, accounting for changes in grid block net volume will not significantly change the compaction. After this last fifth step the workflow returns to the first step for the next time step.

Again it is important to note that the present rate type isotach compaction model is attempting to mimic the delay and persistence in subsidence rates at the onset and arrest of production, by only considering the reservoir compaction and assuming a purely elastic linear response of the rocks surrounding the reservoir rocks. The creep of a possible visco-elastic salt layer on top of the reservoir might also contribute to the non-linearity in the subsidence [NAM et al., 2015].

4.5 Interpolation

Before translating the pressure depletion between two epochs in term of volume compacting, the pressures must be interpolated to shorter time steps than the epochs of obtained from the reservoir simulation models, which may be typically in the order of years. Therefore an interpolation procedure is required for the bilinear, the time decay and the rate type compaction models of **ESIP**. Between each time step a linear relationship between pressure depletion and compaction is assumed. This is an approximation – the behavior predicted by the bilinear, time decay and rate type compaction models is non-linear – and it calls for a careful choice of the time step size. The optimum time step for the interpolation depends on the compaction model parameters and pressure depletion rate. A time step of 6 months was found suitable for the bilinear and time decay models, but it remains an input of **ESIP** to be specified. The most constraining model is the rate type compaction model and its explicit finite difference scheme which requires a sufficiently short time step in order to obtain a stable solution. Therefore, for the rate type model, the time steps are constrained to be such that the pressure drop between two time steps does not exceed 1 bar in any of the grid blocks of the upscaled coarse 2-D grid.

5 From influence functions to ground motions

In order to propagate the 2-D compaction fields to surface subsidence, one needs to compute influence functions, also called Green functions.

5.1 Exponential influence function

The original form of the exponential influence function of the Knothe's Theory [Knothe, 1953], was developed for flat coal seam, and is given by

$$g_v = \frac{1}{R^2} e^{-\pi \frac{r^2}{R^2}} \quad (18)$$

where R is the influence radius as $R = D \tan(\varphi)$, where D is the reservoir depth in our case, and φ the influence angle. The influence angle is the angle between the vertical axis joining the extracted element at depth to its projection at the surface and the line joining the extracted element at depth to the surface location of the border of the subsidence zone. r defines the radius (i.e. horizontal distance) between the vertical projection of the extracted element at the surface and the surface point where the subsidence is calculated.

The only input required by the user for calculating the exponential Knothe influence function (equation (18)) is the influence angle.

The two drawbacks of this approach are that the physic of the process is missing and that one cannot calculate the horizontal displacement caused by extraction of the element at depth.

5.2 Physic-based influence function

[Geertsma (1973)] provided a linear analytical influence function based on the nucleus of strain concept and assuming the layers over and underlying the reservoir as elastically homogeneous. [Van Opstal (1974)] included the effect of a rigid basement in the shape of the influence function. [Fokker and Orlic (2006)] developed a semi-analytical method for generating influence functions for a cake-layer model with layers with different elastic properties. The semi-analytical approach has the advantage of combining relatively complex sub-surface settings with small computational times, making it suitable for inversion and data assimilation exercises.

AESubs, TNO's standalone software generating influence functions based on the semi-analytical approach developed by [Fokker and Orlic, 2006], has been integrated in **ESIP**. *AESubs* generates vertical and horizontal ground surface displacement profiles (influence functions) for a single compacting "nucleus" located at the reservoir depth, and for a given elasticity profile. Inputs required by the user for running *AESubs* are:

- (i) depth of the nucleus (that is the mean depth of the reservoir),
- (ii) depth of the layer interfaces,
- (iii) Young's modulus E and Poisson's ratio ν of each layer, including the reservoir. In the case of a modeled visco-elastic layer (e.g. mimicking a salt layer), its Maxwell viscosity is also required, and the surface

displacement profiles are calculated for a number of time-steps [Fokker and Orlic, 2006].

The assumption of the linearity for the visco-elasticity is supported by the fact that pressure solution creep is the dominant flow mechanism at low differential stress and moderate temperature ([Spiers et al., 1986], [Spiers and Carter, 1998]), which are the conditions for the salt layers capping the Netherlands gas fields.

The tensor form of the constitutive equation of an isotropic Maxwell material (see also [Ranalli, 1996]) can be written as:

$$\dot{\sigma}_{ij} + \frac{\mu}{\eta} \left(\sigma_{ij} - \frac{1}{3} \sigma_{kk} \delta_{ij} \right) = 2\mu \dot{\epsilon}_{ij} + \lambda \dot{\epsilon}_{kk} \delta_{ij} \quad (19)$$

When the Maxwell viscosity η is infinite, the above equation reduces to the constitutive equation of purely elastic material, the so-called Hooke's law. With Laplace transformation, the constitutive equation (19) is translated into a similar set of equations as for the linear elastic case – but as a function of the Laplace coordinates \mathbf{s} . *AESubs* solves these equations for a number of specific values of \mathbf{s} in the same way as for the purely elastic case, and then transform it back to the time domain in a numerical way.

The rotationally symmetric influence function for the vertical displacement that is generated by *AESubs* is used in **ESIP** in conjunction with the 2-D compaction field, in order to calculate the surface subsidence at all the desired geodetic benchmark locations. Note here that the benchmark locations have been identified and are defined by the geodetic module of **ESIP** described in chapter 8. For each location the subsidence contribution of each compacting grid block is summed as:

$$u_3(x, y) = \sum_i \mathbf{Comp}_i \cdot g_v \left(\sqrt{(x - x_i)^2 + (y - y_i)^2} \right) \quad (20)$$

where \mathbf{Comp}_i the compaction of grid block i during each compaction time step; and g_v the elastic influence function, that is the subsidence profile for 1 m³ compaction volume. From the influence function g_v , which is given at discrete locations, the amount of subsidence at the desired benchmark location (x, y) is obtained by cubic-spline interpolation. The cumulative total subsidence at the selected benchmark locations can be derived by the sum of each individual subsidence amounts due to each compacting steps.

In the case of the presence of a visco-elastic layer, the contribution of each past period of compaction are convolved as:

$$u_3(x, y, t) = \sum_i \sum_t \mathbf{Comp}_{i,t} \cdot f_v \left(\sqrt{(x - x_i)^2 + (y - y_i)^2}, t \right) \quad (21)$$

with $\mathbf{Comp}_{i,t}$ the compaction of grid block i during each compacting time steps; the visco-elastic influence function f_v is both location dependent and time dependent.

For one (x, y) benchmark location the convolution scheme can be detailed as:

$$\begin{aligned} u_3(\mathbf{t}_{0,0}) &= \mathbf{0} \\ u_3(\mathbf{t}_{1,0}) &= u_3(\mathbf{t}_{1,0}) + u_3(\mathbf{t}_{0,1}) \\ u_3(\mathbf{t}_{2,0}) &= u_3(\mathbf{t}_{2,0}) + u_3(\mathbf{t}_{1,2}) + u_3(\mathbf{t}_{0,2}) \end{aligned}$$

$$\mathbf{u}_3(\mathbf{t}_{3,0}) = \mathbf{u}_3(\mathbf{t}_{3,0}) + \mathbf{u}_3(\mathbf{t}_{2,3}) + \mathbf{u}_3(\mathbf{t}_{1,3}) + \mathbf{u}_3(\mathbf{t}_{0,3})$$

·
·
·

where $\mathbf{u}_3(\mathbf{t}_{3,0})$ denotes the total subsidence at \mathbf{t}_3 which is the collective sum of:

- (i) $\mathbf{u}_3(\mathbf{t}_{3,0})$: the instantaneous subsidence due to the compaction of each i grid block during the time period $\mathbf{t}_3 - \mathbf{t}_2$.
- (ii) $\mathbf{u}_3(\mathbf{t}_{2,3})$: the subsidence contribution due to the past compaction of each i grid block during the time period $\mathbf{t}_2 - \mathbf{t}_1$.
- (iii) $\mathbf{u}_3(\mathbf{t}_{1,3})$: the subsidence contribution due to the past compaction of each i grid block during the time period $\mathbf{t}_1 - \mathbf{t}_0$.
- (iv) $\mathbf{u}_3(\mathbf{t}_{0,3})$: the subsidence contribution due to the past compaction of each i grid block at \mathbf{t}_0 , which is zero.

As for the location, f_v is time-interpolated following a cubic-spline scheme in order to get the amount of subsidence at the right compacting time step.

It is important to note here that the same procedure is followed for determining the cumulative horizontal displacements, \mathbf{u}_1 (E-W component) and \mathbf{u}_2 (N-S component), from the rotationally symmetric elastic g_h and visco-elastic f_h influence functions. As an example, for a sub-surface layer-cake purely elastic:

$$\mathbf{u}_1(x, y) = \sum_i \mathbf{Comp}_i \cdot \frac{g_h(\sqrt{(x-x_i)^2+(y-y_i)^2})}{\sqrt{(x-x_i)^2+(y-y_i)^2} / (x-x_i)} \quad (22)$$

$$\mathbf{u}_2(x, y) = \sum_i \mathbf{Comp}_i \cdot \frac{g_h(\sqrt{(x-x_i)^2+(y-y_i)^2})}{\sqrt{(x-x_i)^2+(y-y_i)^2} / (y-y_i)} \quad (23)$$

where \mathbf{u}_1 and \mathbf{u}_2 refer respectively to the E-W and N-S horizontal components, positive toward the North and East.

In one of the subsequent steps of **ESIP**, these modelled ground motions will be confronted with observations. Therefore, these calculation results will have to be linearly interpolated from the timings of the reservoir simulation results to the specific times of the geodetic campaigns. The timings of the geodetic campaigns are provided by the geodetic module of **ESIP** described in chapter 8. After time interpolation and for each type of compaction model we have estimated cumulative subsidence and horizontal displacements for the desired benchmarks locations and for the desired timing of geodetic campaigns.

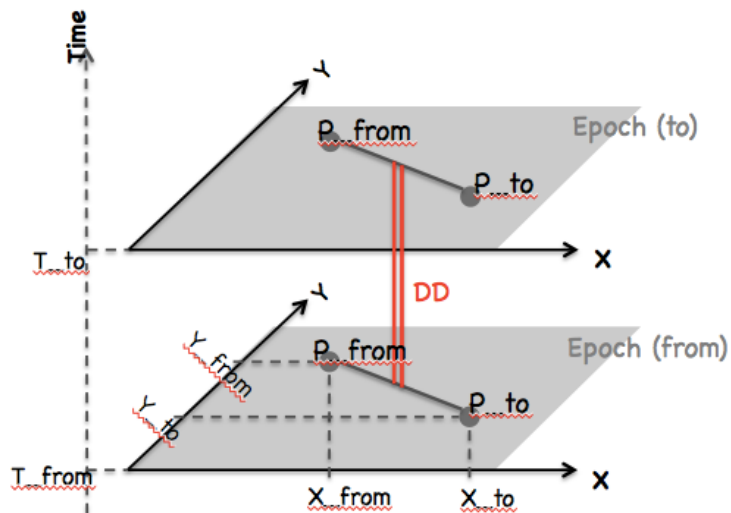
6 Double differences

From the modelled ground motions, double differences **dd** are generated. A double difference indicates a difference in time of a difference in space; in the case of subsidence it can be written as:

$$dd = [u_3(x_1, y_1, t_1) - u_3(x_0, y_0, t_1)] - [u_3(x_1, y_1, t_0) - u_3(x_0, y_0, t_0)] \quad (24)$$

As well this is being visualized in Figure 2.

Concept of double differences



$$DD_OBS = \underbrace{(H_{P_{to}}^{T_{to}} - H_{P_{from}}^{T_{to}})}_{\Delta H^{T_{to}}} - \underbrace{(H_{P_{to}}^{T_{from}} - H_{P_{from}}^{T_{from}})}_{\Delta H^{T_{from}}}$$

H_p^T is the height of benchmark P at epoch T

Figure 2: Concept of double differences

Note here that the same approach is followed for the double differences of horizontal displacements. Again the possible combinations of double differences from the benchmark locations and timing of geodetic campaigns are constrained by the geodetic module of **ESIP**, described in chapter 8.

7 Generating the prior ensemble

Each type of compaction model includes different driving input parameters, which can be adjusted to fit the observations. For example, the time decay compaction model requires two parameters, C_m and τ (see chapter 4 for more details about the other type of compaction model). In the same way, influence functions generated by *AEsubs* require input parameters characterizing the elastic and visco-elastic properties (Young's modulus E , Poisson's ratio ν , Maxwell's viscosity η) of each layer of the subsurface. As an example, one can take the time decay compaction model and a three-layer subsurface elastic model. In this case, 8 driving input parameters are needed for running the geomechanical forward model: C_m and τ for the reservoir compaction, and elastic modulus E and Poisson's ratio ν for each subsurface layer.

Parameters of the compaction models and those of the influence functions are gathered together as parameters of the geomechanical forward model followed in the *ESIP* workflow. A-priori knowledge regarding each of these driving input parameters are in the form of their statistical distributions (e.g. normal, uniform, triangular). A different type of statistical distribution can be chosen for each parameters.

Ensembles of prior ground motion predictions are generated by stochastically selecting values in the prior distributions of the driving input parameters of the geomechanical forward model. This is being performed via a specific sampling scheme and which is described in a confidential Appendix to this report and which is not being provided with the open version of this report.

When the sampling procedure has been performed one can generate the prior ensemble of N_e ground motions predictions. This procedure can be done for each type of compaction model. More precisely, for each type of compaction models, the prior ensemble for each type of ground motions (\mathbf{u}_3 , \mathbf{u}_1 , \mathbf{u}_2), and the prior ensemble of double differences are generated.

8 Geodetic data

The modelled double differences, which can be seen as prior predictions, will be later on refined by the conditioning steps with the geodetic data. This conditioning step model/data will be presented below in chapter 9, here we present the procedure to obtain the geodetic data. Currently, two types of geodetic data can be handled: levelling and GPS.

The **ESIP** module that performs the geodetic data handling has been developed by TU Delft as part of a separate assignment for NAM and is further described in [Van Leijen et al., 2017]. This module has been integrated as standalone module in **ESIP** and can be applied on specific geodetic databases for the Netherlands not all brought to the attention of TNO. The main user input contains

- (i) the geographical coordinates of the polygon of interest (supposedly on top of the gas field of interest but not limited to that), and
- (ii) the time interval of interest, a set of double differences and their associated covariance matrix are automatically generated.

The algorithm looks for all the possible combinations of double differences for each type of geodetic data, and generates a set of double differences and their associated covariance matrix. The covariance matrix of the double differences gives the uncertainty/variance of each measurement but also the spatiotemporal correlations between each measurement. More background on this module of **ESIP**, not developed by TNO, and the specific approaches applied can be found in [Van Leijen et al., 2017] .

9 Conditioning of the models with the data

The main aspect of the Bayesian based workflow of **ESIP** is to take advantage of (i) a-priori knowledge, and (ii) ground motions data from time T_0 to T_1 in order to predict the surface subsidence at time T_2 assuming a production/depletion scenario from T_1 to T_2 .

For each type of compaction model, **ESIP** first creates a prior model vector ensemble of N_e vectors $\mathbf{M}_0 = (\mathbf{m}_1, \mathbf{m}_2, \dots, \mathbf{m}_{N_e})$ based on our prior information. These vectors are generated by stochastically selecting values in the prior distributions of the driving input parameters, and in this sense our a-priori knowledge has been mapped to the reservoir model driving input parameters and those of the geomechanical forward model.

Secondly from our a-priori knowledge one can generate an ensemble \mathbf{GM}_0 of ground motion predictions (mostly including surface subsidence) and double differences for each type of compaction model via the influence function in the geomechanical forward model. The geomechanical forward model is indicated by the function \mathbf{G} working on each vector of prior model parameters.

It is important to bear in mind here that the double differences predictions are directly derived from the ground motion predictions and in this sense include the same information. For the sake of clarity, the ensembles \mathbf{GM}_0 for each type of compaction model, will from now on only refer to the ensemble of N_e prior double difference predictions:

$$\mathbf{dd}^{prior} = (\mathbf{dd}_1^{prior}, \mathbf{dd}_2^{prior}, \dots, \mathbf{dd}_{N_e}^{prior}). \quad (25)$$

For each type of compaction models one can define a mean and a covariance matrix of the prior double differences predictions. The mean over the N_e members is defined as:

$$\langle \mathbf{GM}_0 \rangle = \mu[\mathbf{dd}^{prior}] = \frac{1}{N_e} \sum_{i=1}^{N_e} \mathbf{dd}_i^{prior} \quad (26)$$

The covariance over the N_e members between the j th location and the k th location being defined by the following covariance matrix:

$$c_{jk}^{prior} = \frac{1}{N_e - 1} \sum_{i=1}^{N_e} (\mathbf{dd}_{ij}^{prior} - \mu[\mathbf{dd}_j^{prior}]) \cdot (\mathbf{dd}_{ik}^{prior} - \mu[\mathbf{dd}_k^{prior}]) \quad (27)$$

which can be written in matrix notation as:

$$\mathbf{C}^{prior} = (\mathbf{GM}'_0 \cdot \mathbf{GM}'_0^T) / (N_e - 1) \quad (28)$$

And where

$$\mathbf{GM}'_0 = \mathbf{GM}_0 - \langle \mathbf{GM}_0 \rangle. \quad (29)$$

The 4 mean priors $\langle \mathbf{GM}_0 \rangle$ calculated for the 4 compaction model types can be seen as our best prior estimates.

Consequently from now, only considering our prior knowledge (and assuming a production scenario from time \mathbf{T}_1 to \mathbf{T}_2), one can generate 4 best prior estimates for the 4 types of compaction model from \mathbf{T}_0 to \mathbf{T}_2 .

For a real scenario time \mathbf{T}_1 and \mathbf{T}_2 will correspond respectively to the present day and a future geodetic campaign. For a synthetic scenario time \mathbf{T}_1 can be theoretically picked up anytime between \mathbf{T}_0 and \mathbf{T}_2 ; this allows testing of the robustness of the workflow and its sensitivity to different choices made in running it.

The next step corresponds to confront or condition the prior estimates up to \mathbf{T}_1 with the geodetic data acquired up to \mathbf{T}_1 . The goal here is to take advantage of the ground motions measurements up to \mathbf{T}_1 in order to refine our predictions. The next paragraphs will document two approaches for the evaluation against the measurements: the Red-Flag [Nepveu et al., 2010] and Ensemble Smoother (e.g. [Fokker et al., 2016]) approach.

9.1 Red-Flag approach

For a particular realization \mathbf{r} of the ensemble \mathbf{GM}_0 , the Red-Flag approach defines the mismatch function as:

$$I(\mathbf{r}) = \frac{1}{2N} (\mathbf{dd}_r^{\text{prior}} - \mathbf{dd})^T \mathbf{C}_{dd}^{-1} (\mathbf{dd}_r^{\text{prior}} - \mathbf{dd}) \quad (30)$$

with N the number of double differences from \mathbf{T}_0 to \mathbf{T}_1 of the vector data \mathbf{dd} and prior model $\mathbf{dd}_r^{\text{prior}}$. The lower the value of the mismatch function, the better the match of the vector of prior double difference predictions with the measurements. In this formulation, \mathbf{C}_{dd} represents the covariance matrix of the measurements. It is usually assumed that the non-diagonal values vanish – that is the different data points are uncorrelated. Instead, in our workflow, the full \mathbf{C}_{dd} covariance matrix (generated by the geodetic module of **ESIP**) is taken into account. Also the relative importance (~weight) of the different data points is handled by \mathbf{C}_{dd} : points with a larger variance receive less weight.

The mismatch function (29) can be read as the Gaussian likelihood of the data, that is:

$$P(\mathbf{dd} | \mathbf{dd}_r^{\text{prior}}) = \exp[-I(\mathbf{r})]. \quad (31)$$

The Bayesian probability of a particular realization \mathbf{r} of the ensemble is thus given as

$$P(\mathbf{dd}_r^{\text{prior}} | \mathbf{dd}) = \frac{P(\mathbf{dd}_r^{\text{prior}}) \cdot P(\mathbf{dd} | \mathbf{dd}_r^{\text{prior}})}{\sum_{i=1}^{N_e} P(\mathbf{dd}_i^{\text{prior}}) \cdot P(\mathbf{dd} | \mathbf{dd}_i^{\text{prior}})}. \quad (32)$$

In the right-hand side of the numerator, we have the prior probability of the realization (i.e. $1/N_e$) before confrontation with the measurements, and the

associated likelihood of the data. The denominator is a normalizing factor, in order for the sum of all the $P(\mathbf{d}\mathbf{d}_r^{prior}|\mathbf{d}\mathbf{d})$ to be equal to one.

The model probability $P(\mathbf{d}\mathbf{d}_r^{prior}|\mathbf{d}\mathbf{d})$ based on the confrontation between model and measurements up to time \mathbf{T}_1 , is used in a direct way to assign a weight $\mathbf{w}_r = P(\mathbf{d}\mathbf{d}_r^{prior}|\mathbf{d}\mathbf{d})$ to every model realizations computed up to time \mathbf{T}_1 . The same weights based on the confrontation between model and measurements up to time \mathbf{T}_1 can be also assigned to every model realization computed up to time \mathbf{T}_2 (date of a future geodetic campaign). The last step consists in computing the weighted mean and weighted covariance matrix of the posterior double differences prediction both up to \mathbf{T}_1 and up to \mathbf{T}_2 as it follows:

$$\boldsymbol{\mu}[\mathbf{d}\mathbf{d}^{post}] = \mathbf{w} \cdot \mathbf{GM} = \sum_{i=1}^{N_e} \mathbf{w}_i \mathbf{d}\mathbf{d}_i^{prior} \quad (33)$$

$$\mathbf{c}_{jk}^{post} = \frac{1}{1 - \sum_{i=1}^{N_e} \mathbf{w}_i^2} \sum_{i=1}^{N_e} \mathbf{w}_i (\mathbf{d}\mathbf{d}_{ij}^{prior} - \boldsymbol{\mu}[\mathbf{d}\mathbf{d}_j^{post}]) (\mathbf{d}\mathbf{d}_{ik}^{prior} - \boldsymbol{\mu}[\mathbf{d}\mathbf{d}_k^{post}]) \quad (34)$$

where \mathbf{c}_{jk}^{post} is the posterior covariance between the j^{th} location and the k^{th} location; and which can be written in matrix notation as:

$$\mathbf{C}^{post} = (\mathbf{GM}'^T \cdot (\mathbf{w} \cdot \mathbf{GM}'')) / (1 - \sum_{i=1}^{N_e} \mathbf{w}_i^2) \quad (35)$$

where

$$\mathbf{GM}'' = \mathbf{GM} - (\mathbf{w} \cdot \mathbf{GM}). \quad (36)$$

At this stage, following the Red-Flag confrontation approach, one computed the weighted mean and weighted covariance matrix of the posterior double differences prediction both up to \mathbf{T}_1 and up to \mathbf{T}_2 and for each type of compaction model.

Before switching to the next confrontation approach, note here that with the model weights \mathbf{w} based on the confrontation between prior double differences and measurements up to time \mathbf{T}_1 , one can also calculate the mean ground motions $\boldsymbol{\mu}[\mathbf{d}^{post}]$ (where \mathbf{d}^{post} here represents the posterior $\mathbf{u}_3, \mathbf{u}_1, \mathbf{u}_2$), and their associated standard deviation $\boldsymbol{\sigma}[\mathbf{d}^{post}]$ for each benchmark locations and for each timing of geodetic campaigns between \mathbf{T}_0 to \mathbf{T}_2 as:

$$\boldsymbol{\mu}[\mathbf{d}^{post}] = \sum_{i=1}^{N_e} \mathbf{w}_i \mathbf{d}_i^{prior} \quad (37)$$

$$\boldsymbol{\sigma}[\mathbf{d}^{post}] = \sqrt{\frac{\sum_{i=1}^{N_e} \mathbf{w}_i (\mathbf{d}_i^{prior} - \boldsymbol{\mu}[\mathbf{d}^{post}])^2}{\frac{(l-1)}{l}}} \quad (38)$$

where \mathbf{d}^{prior} denotes the prior ground motions ($\mathbf{u}_3, \mathbf{u}_1, \mathbf{u}_2$) between \mathbf{T}_0 to \mathbf{T}_2 ; and l is the number of non-zero weights \mathbf{w} .

9.2 Ensemble Smoother approach

The Ensemble Smoother approach consists in an inversion scheme, for which the goal is to maximize (or minimize $-\log[\mathcal{J}]$) an objective function of the form (see [Menke, 1989], [Tarantola, 2005]):

$$J(\mathbf{m}) = \exp\left[-\frac{1}{2}((\mathbf{G}(\mathbf{m}) - \mathbf{dd})^T \mathbf{C}_{dd}^{-1} (\mathbf{G}(\mathbf{m}) - \mathbf{dd}) + (\mathbf{m} - \mathbf{m}_0)^T \mathbf{C}_m^{-1} (\mathbf{m} - \mathbf{m}_0))\right] \quad (39)$$

where \mathbf{m} and $\mathbf{G}(\mathbf{m})$ are respectively the “optimized” (posterior) vector of model parameters and double differences predictions (that is \mathbf{dd}^{post}) from time \mathbf{T}_0 to \mathbf{T}_1 . More specifically \mathbf{m} represents the updated “optimized” (posterior) driving input parameters of the geomechanical forward model (e.g. $\mathbf{C}_{m_{pre}}$, $\mathbf{C}_{m_{post}}$, \mathbf{P}_{trans} for the bilinear compaction model). Following this approach the objective function is integrated in an inversion scheme seeking the solution for the vector \mathbf{m} of model parameters that optimize the match with data and with prior information \mathbf{m}_0 . This way, the Ensemble smoother conditioning step updates both models and predictions; instead Red-Flag adjusts model weights according to the data. Beside the fact that the Ensemble Smoother includes an inversion exercise and Red-Flag does not; the main difference between the two methods for confronting model with data is that for the Ensemble smoother we explicitly include our prior knowledge \mathbf{m}_0 and the model covariance matrix \mathbf{C}_m (explained in the sequel of this section) with the term $(\mathbf{m} - \mathbf{m}_0)^T \mathbf{C}_m^{-1} (\mathbf{m} - \mathbf{m}_0)$. For the Red-Flag mismatch function, our prior knowledge is implicitly included in \mathbf{dd}^{prior} .

Following the Ensemble Smoother approach, we take advantage of the prior knowledge (coming from previous studies) on the statistical distributions of each model parameter (such as permeability, porosity, compaction coefficients...). The Ensemble Smoother objective function (39) stresses the relative importance of the different prior model parameters (certain parameters receive less weight through a larger variance); it correctly weighs parameters and measurements (by the relative magnitude of \mathbf{C}_{dd} and \mathbf{C}_m); it correctly incorporates correlations between prior model parameters and between different measurement values (by the non-diagonal elements in \mathbf{C}_{dd} and \mathbf{C}_m). If one parameter has no clear definite knowledge/belief, its variance should be larger. For the extreme case that none of the model parameters are well defined/known, the \mathbf{C}_m values should be extremely large and the term $(\mathbf{m} - \mathbf{m}_0)^T \mathbf{C}_m^{-1} (\mathbf{m} - \mathbf{m}_0)$ in equation (39) can be neglected. Although the density of measurements above some areas of a field can be small, their influence can still be substantial through a variability of the prior model parameters that specifically affects the match with those measurements while much less influencing the match with the more dense measurements. For instance, if there are only few measurements above an aquifer with uncertain properties, the variability of the aquifer properties can be reduced by the measurements while the influence on the gas-bearing part – where the measurements are denser – is only limited.

The optimal “least-square” solution of (39) for one particular realization of the ensemble and assuming a linear inverse problem is given by:

$$\hat{\mathbf{m}} = \mathbf{m}_0 + \mathbf{C}_m \mathbf{G}^T (\mathbf{G} \mathbf{C}_m \mathbf{G}^T + \mathbf{C}_{dd})^{-1} (\mathbf{dd} - \mathbf{G} \mathbf{m}_0) . \quad (40)$$

For an ensemble-based estimate with a non-linear problem we define \mathbf{GM}_0 as the result of the non-linear geomechanical forward model working on all the members of the ensemble, that is the ensemble of prior double differences predictions from \mathbf{T}_0 to \mathbf{T}_1 . For an ensemble-based estimate, the Ensemble Smoother then gives as updated model parameter ensemble:

$$\widehat{\mathbf{M}} = \mathbf{M}_0 + \mathbf{M}'_0 [\mathbf{G}\mathbf{M}'_0]^T \{ \mathbf{G}\mathbf{M}'_0 [\mathbf{G}\mathbf{M}'_0]^T + (N_e - 1) \mathbf{C}_{dd}^{-1} \}^{-1} \times (\mathbf{D}\mathbf{D} - \mathbf{G}\mathbf{M}_0) \quad (41)$$

with $\mathbf{G}\mathbf{M}_0$, as before for Red-Flag, represents the result of the non-linear geomechanical forward model working on all the members of the ensemble, that is the ensemble of prior double differences predictions from \mathbf{T}_0 to \mathbf{T}_1 . This expression uses the expression for the empirically estimated model covariance matrix $\mathbf{C}_m = \frac{\mathbf{M}'_0 \mathbf{M}'_0{}^T}{N_e - 1}$ for the ensemble of model realizations. The estimate for \mathbf{C}_m includes the known and belief bandwidths of the model parameters. Clearly, the larger the ensemble, the better the numerical estimate of the \mathbf{C}_m should be. Primes in Eq. (41) indicate anomalies with respect to the ensemble mean as $\mathbf{M}'_0 = \mathbf{M}_0 - \langle \mathbf{M}_0 \rangle$. Finally $\mathbf{D}\mathbf{D} = (\mathbf{d}\mathbf{d} + \varepsilon_1, \mathbf{d}\mathbf{d} + \varepsilon_2, \dots, \mathbf{d}\mathbf{d} + \varepsilon_{N_e})$ corresponds to an ensemble of double differences data realizations created adding to the vector data $\mathbf{d}\mathbf{d}$ different random noise vectors ε that lie within the uncertainty range of the measurements. This procedure ensures a posterior error covariance that is consistent with the theory.

Ideally the reservoir model should be run again with the new updated model parameters $\widehat{\mathbf{M}}$ to create new pressure distributions up to time \mathbf{T}_2 before running again the geomechanical forward model. However as a first approximation and assuming linearity, one can directly include in \mathbf{M}_0 :

- the prior double differences from \mathbf{T}_0 to \mathbf{T}_1 ,
- the prior double differences from \mathbf{T}_0 to \mathbf{T}_2 ,
- the prior ground motions ($\mathbf{u}_3, \mathbf{u}_1, \mathbf{u}_2$) predictions from \mathbf{T}_0 to \mathbf{T}_2 .

This way one can update in one single step:

- all the model parameters with
- the prior double differences predictions from \mathbf{T}_0 to \mathbf{T}_1 ,
- the prior double differences predictions from \mathbf{T}_0 to \mathbf{T}_2 ,
- the prior ground motions predictions from \mathbf{T}_0 to \mathbf{T}_2 .

In other words, in doing so $\widehat{\mathbf{M}}$ includes now:

- the posterior model parameters,
- the posterior double differences predictions from \mathbf{T}_0 to \mathbf{T}_1 ,
- the posterior double differences predictions from \mathbf{T}_0 to \mathbf{T}_2 ,
- the posterior ground motions ($\mathbf{u}_3, \mathbf{u}_1, \mathbf{u}_2$) predictions from \mathbf{T}_0 to \mathbf{T}_2 .

From the ensemble of posterior double differences predictions $\widehat{\mathbf{G}\mathbf{M}}$ (now embedded in $\widehat{\mathbf{M}}$), the posterior mean double differences predictions over all the ensemble members $\langle \widehat{\mathbf{G}\mathbf{M}} \rangle$ and the posterior covariance matrix $\mathbf{C}_{\widehat{\mathbf{G}\mathbf{M}}}$ can be computed as:

$$\langle \widehat{\mathbf{G}\mathbf{M}} \rangle = \mu[\mathbf{d}\mathbf{d}^{post}] = \frac{1}{N_e} \sum_{i=1}^{N_e} \mathbf{d}\mathbf{d}_i^{post} \quad (42)$$

$$\mathbf{C}_{\widehat{\mathbf{G}\mathbf{M}}} = \frac{[\widehat{\mathbf{G}\mathbf{M}}][\widehat{\mathbf{G}\mathbf{M}}]^T}{N_e - 1}. \quad (43)$$

The mean and covariance matrix of the posterior double differences prediction both up to \mathbf{T}_1 and up to \mathbf{T}_2 and for each type of compaction model can thus be computed.

One can also extract from $\widehat{\mathbf{M}}$ the ensemble of posterior ground motions ($\mathbf{u}_3, \mathbf{u}_1, \mathbf{u}_2$) predictions from \mathbf{T}_0 to \mathbf{T}_2 , and one can calculate the means of the ground motions and their attached standard deviations at each benchmark locations and for each timing of geodetic campaigns between \mathbf{T}_0 to \mathbf{T}_2 as:

$$\mu[\mathbf{d}^{post}] = \frac{1}{N_e} \sum_{i=1}^{N_e} \mathbf{d}_i^{post} \quad (44)$$

$$\sigma[\mathbf{d}^{post}] = \sqrt{\frac{1}{N_e-1} \sum_{i=1}^{N_e} (\mathbf{d}_i^{post} - \mu[\mathbf{d}^{post}])^2} . \quad (45)$$

10 Assessment

For both the Red-Flag and Ensemble Smoother approach, of **ESIP** computes 4 posterior means and their attached covariance matrix for each type of compaction model. Consequently, 8 updated models are now available and it remains to judge whether the method has worked properly (and possibly decide for the determination of the model that is best fitting the data). To this aim, one can use the χ^2 method. The number calculated in this method judges if the model posterior predictions and the data are consistent: their average mismatch should be of order unity. In this number, a combination of the data covariance and the covariance of the posterior prediction must be employed:

$$\chi_{red}^2 = \frac{1}{\nu} (\mathbf{dd} - \boldsymbol{\mu}[\mathbf{dd}^{post}])^T \cdot [\mathbf{C}_{dd} + \mathbf{C}_{GM}]^{-1} \cdot (\mathbf{dd} - \boldsymbol{\mu}[\mathbf{dd}^{post}]) \quad (46)$$

where ν is the number of degree of freedom given as $N_{dd} - n_f$ with N_{dd} the number of double differences and n_f the number of model parameters. The χ^2 method takes into consideration the model complexity, that is a model with more degrees of freedom (e.g. the rate type compaction model) will be penalized. Here, $\chi_{red}^2 = 1$ means that model is matching the data and that the quality of the match is in agreement with the error covariance of the data. If $\chi_{red}^2 \gg 1$, it means that either the model is poorly fitting the data or the covariance of the data has been underestimated. If $\chi_{red}^2 > 1$, it means that the model is fairly close to the data and that the mismatch is either due to the model or again that the covariance of the data has been underestimated. When $\chi_{red}^2 < 1$, it means that the model is “over-fitting” the data, which can be due to the model but also again can be due to an overestimation of the covariance of the data.

It is not straightforward to use χ_{red}^2 for the assessment of a model performance, or to distinguish between models. The χ_{red}^2 assessment is primarily on the performance of the method. It can happen that a poor model can still give a reasonable value for χ_{red}^2 because the posterior covariance is still large. The question on selection of the right conceptual model using the data is related to the concept of *observability*. More research is required to apply such concepts to the problem at hand.

11 References

- Bjerrum, L., 1967, Engineering Geology of Norwegian Normally Consolidated Marine Clays as Related to the Settlements of Buildings, *Geotechnique*, 17, pp 81-118.
- De Waal, J.A., 1986. On the rate type compaction behaviour of sandstone reservoir rock. doctoral thesis.
<http://repository.tudelft.nl/islandora/object/uuid:b805782b-2eb4-4f72-98f4-f727c4ea9df0?collection=research>
- Doornhof, D., 1992. Surface subsidence in The Netherlands: The Groningen gas field. *Geol. Mijnbouw* 71, 119–130.
- E.J. den Haan, Het, 2003. a,b,c – Isotachenmodel: hoeksteen van een nieuwe aanpak van zettingsberekeningen, *Geotechniek*.
- Emerick, A. A. and Reynolds, A. C., 2013. Ensemble smoother with multiple data assimilation. *Computers & Geosciences*, 55:3–15.
- Evensen, G., 2003. The Ensemble Kalman Filter: theoretical formulation and practical implementation, *Ocean Dynamics*, 53: 343. doi:10.1007/s10236-003-0036-9.
- Fokker, P.A., Orlic, B., 2006. Semi-Analytic Modelling of Subsidence. *Mathematical Geology*, Vol. 38, No. 5, July 2006. DOI: 10.1007/s11004-006-9034-z
- Fokker, P.A., Wassing, B.B.T., van Leijen, F.J., Hanssen, R.F., Nieuwland, D.A., 2016. Application of an ensemble smoother with multiple data assimilation to the Bergermeer gas field, using PS-InSAR. *Geomechanics for Energy and the Environment*, Vol. 5, No. March, 2016, p. 16-28.
- Geertsma, J., 1973). Land Subsidence Above Compacting Oil and Gas Reservoirs, *J. Petr. Tech.*, pp.734-744.
- Jaynes ET, 2003. Probability theory. The logic of science. Cambridge University Press, Cambridge
- Knothe S., 1953. Równanie ostatecznie wykształconej niecki osiadania. *Archiwum Górnictwa i utnictwa*, tom 1, z.1, 1953. (Equation of a finally developed depression. In: *Mining and Metallurgy Archives*, vol. 1, bul. 1)
- Menke, W., 1989. *Geophysical Data Analysis: Discrete Inverse Theory*, revised edition, San Diego: Academic Press.
- Mossop, A., 2012. An explanation for anomalous time dependent subsidence, 46th US Rock Mechanics/Geomechanics Symposium, Chicago, Illinois, USA, 24–27 June 2012, 12-518.
- NAM et al., 2015. Long Term Subsidence Study
<http://www.waddenacademie.nl/en/themes/geoscience/scientific-steering-committee-subsidence/>

Nepveu M., Kroon, I. C., Fokker, P. A., 2010. Hoisting a Red Flag: An Early Warning System for Exceeding Subsidence Limits. *Mathematical Geosciences*. February 2010, Volume 42, Issue 2, pp 187–198.

Pruiksma, J., Breunese, J. N., van Thienen-Visser, K., and de Waal, J. A.: Isotach formulation of the Rate Type Compaction Model for sandstone, 2015. *Int. J. Rock Mech.*, 78, 127–132.

Ranalli, G., 1996. *Rheology of the Earth*, Allen and Unwin, St Leonards, N.S.W., Australia.

Reggiani P, Weerts AH, 2008. A Bayesian approach to decision-making under uncertainty: an application to real-time forecasting in the river Rhine. *J Hydrol* 356:56–69.

Spiers, C.J., Urai, J.L., Lister, G.S., Boland, J.N., Zwart, H.J., 1986. The influence of fluid–rock interaction on the rheology of salt rock. EUR 10399 EN, Office for Official Publications of the European Communities, Luxembourg, 131 pp.

Spiers, C.J. & Carter, N.L., 1998. Microphysics of rocksalt flow in nature. In: M. Aubertin & H.R.Hardy (Eds.) *The Mechanical Behaviour of Salt: Proceedings of the Fourth Conference Series on Rock*.

Tarantola, A., 2005. *Inverse Problem Theory and Methods for Model Parameter Estimation*. Society for Industrial and Applied Mathematics.

Thienen-Visser, K. van, Nepveu, M., Hettelaar, J.M.M., 2012. Deterministische hazard analyse voor geïnduceerde seismiciteit in Nederland, TNO-rapport 2012 R10198.

Thienen-Visser, K. van, Pruiksma, J.P., Breunese, J.N., 2015. Compaction and subsidence of the Groningen gas field in the Netherlands, in *Proceeding of IAHS*, 372, 367-373.

Van Leijen, F.J., Samiei Esfahany, S., Van der Marel, H., Hanssen, R.F., 2017. Uniformization of Geodetic data for deformation analysis. Contribution to the research project: Second phase of the long-term subsidence study in the Wadden Sea region (LTS2). TU Delft, final report, v1.0

Van Opstal, G., 1974. The effect of base-rock rigidity on subsidence due to reservoir compaction, in *Advances in rock mechanics*, 3rd congress Denver.

Confidential Appendix: Sampling scheme

< Intentionally left blank for distribution of main part of report due to confidential character of contents of Appendix >